УДК 533.93:537.525
P.A.C.S. 52.40.Hf; 61.72.Ww; 68.55.Ln; 79.20.Rf
DOI 10.54708/26587572_2023_5313131

STUDY OF THE SYNERGY EFFECT OF HIGH-INTENSITY ALUMINUM IONS IMPLANTATION INTO TITANIUM AND ENERGY IMPACT ON THE SURFACE

Alexander Ilyich Ryabchikov [1], Olga Sergeevna Korneva [1a], Irina Alexandrovna Kurzina [2], Vladislav Aleksandrovich Tarbokov [1]

[1] National Research Tomsk Polytechnic University, 30 Lenin Ave., 634050, Tomsk, Russia
[2] National Research Tomsk State University 36 Lenin Ave., 634050, Tomsk, Russia
[a] oskar@tpu.ru

ABSTRACT

The work studies the synergy effect of high-intensity implantation of aluminum ions and the subsequent impact of a powerful pulsed ion beam on the microstructure and properties of titanium. Specimens of titanium were implanted for one hour at a temperature of 1170 K with an ion fluence of 10^{21} ions/cm^2. Layers with a thickness of about 150 μm were obtained. The energy impact was carried out by a powerful nanosecond pulsed ion beam with an ion current density on the target of 100 A/cm^2. The paper presents data on changes in the elemental composition, surface morphology, and microstructure of ion-doped and energy-modified layers. It has been established that the additional energy impact on the ion-doped layer of a powerful pulsed beam improves microstructure at depths greater than 3.4 μm. The synergistic of high-intensity ion implantation of aluminum and the energy impact of a pulsed ion beam improves the wear resistance of titanium by eighteen folds.

KEYWORDS

Vacuum arc; plasma; high intensity; ion implantation; energy impact; synergy effect.

ИССЛЕДОВАНИЕ СИНЕРГИИ ВЫСОКОИНТЕНСИВНОЙ ИМПЛАНТАЦИИ ИОНОВ АЛЮМИНИЯ В ТИТАН И ЭНЕРГЕТИЧЕСКОГО ВОЗДЕЙСТВИЯ НА ПОВЕРХНОСТЬ

Александр Ильич Рябчиков [1], Ольга Сергеевна Корнева [1a], Ирина Александровна Курзина [2], Владислав Александрович Тарбоков [1]

[1] Национальный исследовательский Томский политехнический университет, Россия, 634050, Томск, пр. Ленина, 30
[2] Национальный исследовательский Томский государственный университет, Россия, 634050, Томск, пр. Ленина, 36
[a] oskar@tpu.ru

АННОТАЦИЯ

В работе исследована синергия высокоинтенсивной имплантации ионов алюминия и последующего воздействия мощного импульсного ионного пучка на микроструктуру и свойства титана. Образцы титана имплантировали один час при температуре 1170 К с флюенсом ионов 10^{21} ион/см^2. Были получены слои толщиной около 150 мкм. Энергетическое воздействие осуществлялось мощным наносекундным импульсным ионным пучком с плотностью ионного

тока на мишени 100 А/см^2. В работе представлены данные об изменении элементного состава, морфологии поверхности и микроструктуры ионно-легированных и энергомодифицированных слоев. Установлено, что дополнительное энергетическое воздействие на ионно-легированный слой мощного импульсного пучка улучшает микроструктуру на глубину более 3,4 мкм. Синергия высокоинтенсивной ионной имплантации алюминия и энергетическое воздействие импульсного ионного пучка повышает износостойкость титана в восемнадцать раз.

КЛЮЧЕВЫЕ СЛОВА

Вакуумная дуга; плазма; высокая интенсивность; ионная имплантация; энергетическое воздействие; синергия.

Introduction

Methods for modifying surface layers by charged particle beams, laser radiation, and high-pulse plasma flows are widely used in many fields of science and technology for directed changes in the physical and mechanical properties of various materials. Various ways and methods are divided into two classes. First one includes the methods that change the elemental composition and microstructure due to ion doping of the target's near-surface layer [1–17]. Second one includes the methods based on the pulsed impact on the surface of energy flows of high power density, which modifies the microstructure of the surface layers due to the effect of superfast heating and cooling of the target's near-surface layer without changing or slightly changing the elemental composition [18–28].

The main problem of ion implantation, which limits its wide application, is related to the low range of ions in a solid. Using the example of nitrogen ion implantation, Wei and other authors demonstrated in their works the possibility of increasing the ion-doped layer depth due to dopant diffusion enhancement with increasing ion current density, which made the ion implantation method for improving the performance properties of metals and alloys more attractive [29–33]. The development of the high-intensity ion implantation method has shown the possibility of forming deep ion-doped layers in metals and alloys during implantation of both gas and metal ions, due to the production and use of repetitively-pulsed gas and metal ion beams with an ion current density increased by several orders of magnitude [34, 35]. It was found that the processes of diffusion and phase formation during the metal ion implantation require high temperatures, which in turn cause the grain structure growth. For example, the work [36] presents the results on the formation of Ti_3Al and TiAl intermetallic phases, as well as solid solutions of various compositions down to a depth of ~50 μm, where the grain sizes of the Ti_3Al phase reach 5 μm or more. This work is devoted to the study of the synergy effects of high-intensity aluminum ion implantation into titanium and energy impact on the surface with an ion beam of superhigh pulse power in order to decrease the grain sizes and improve its microstructure and properties.

1. Experimental Setups

High-intensity implantation of aluminum ions was carried out using an experimental setup equipped with an axially symmetrical vacuum-arc evaporator. The scheme of the experiment is shown in Fig. 1.

The formation of high-intensity aluminum ion beams was carried out by a method based on plasma-immersion extraction of ions from the free plasma boundary, their acceleration in a high-voltage sheath, followed by ballistic focusing [37]. Using the "solar eclipse" effect, the plasma was cleaned from the products of explosive cathode erosion. The samples of commercially pure titanium (grade 2) with the dimensions of 45×25×3 mm were used as targets and mounted in the geometrical focus region of the beam. The initial analysis of the specimens made of titanium demonstrated that alloy had 98.96 at.% of Ti and a low content of Fe, Si and V (0.13, 0.29 and 0.14 at.%, respectively). The specimen surface was pre-polished to the roughness of 100 nm and cleaned with alcohol.

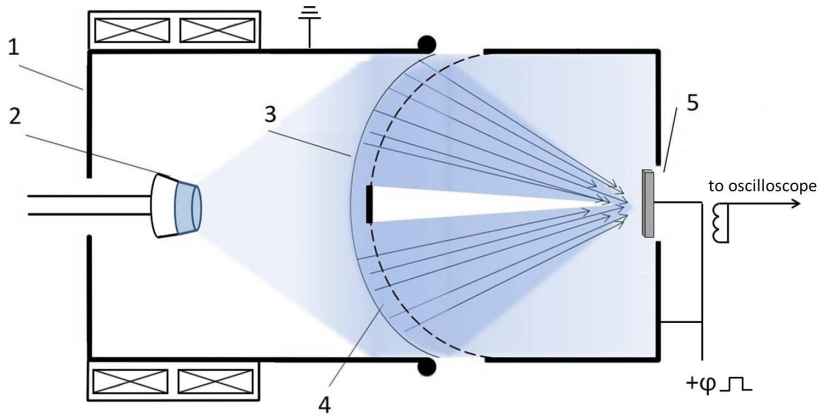

Fig. 1. Scheme of plasma-immersion formation of high intensity aluminum ion beam and implantation of ions into titanium:
1 – anode, 2 – cathode, 3 – ion-emission plasma boundary, 4 – high voltage sheath, 5 – sample-collector

Рис. 1. Схема плазменно-иммерсионного формирования пучка ионов алюминия высокой интенсивности и имплантации ионов в алюминий:
1 – анод, 2 – катод, 3 – ионно-эмиссионная граница плазмы, 4 – слой разделения заряда, 5 – образец-коллектор

Implantation was carried out for one hour at a temperature of 1170 K (the temperature was measured from the target's rear side using an isolated thermocouple) with an irradiation fluence of 10^{21} ions/cm^2. The ion beam was formed at bias potential amplitude of 0.6 kV, a frequency of 40 kHz, and a duty factor of about 65%. Taking into account the average charge state of aluminum ions Z ~1.73 in the vacuum arc discharge plasma, the average energy of the ions slightly exceeded 1 keV [38]. Maintaining a constant temperature during ion implantation was carried out due to varying the frequency of the bias potential pulses.

The energy impact with a high-power ion beam (HIB) was carried out on a TEMP-4M accelerator [1] at an accelerating voltage of 200 kV, a pulse duration at half maximum of 100 ns, and an energy density of 1.5 J/cm^2 (for metallic materials, this is the regime with surface layer melting). The composition of the ion beam is carbon ions (C+, C++) up to 70%, protons – up to 30%. The distance from the ion diode to the treated surface was 15 cm. The pressure in the vacuum chamber was no more than 1×10* (–4) Torr [39].

The distribution of aluminum dopant over the modified layer thickness on a transverse section, made using a Saphir 320 grinding and polishing machine, was carried out using a Hitachi S-3400 N scanning electron microscope equipped with a Bruker XFlash 4010 energy-dispersive attachment. The elemental composition of the test specimens was determined by X-ray microanalysis (MRSA) using an INCA-Energy energy-dispersive X-ray microanalyzer (EDX) (Oxford Instruments) built into a LEOEVO-50XVP scanning electron microscope. The phase composition of the test specimens was analyzed by X-ray phase analysis (XPA) based on the analysis of diffraction pattern obtained using a DRON-7 diffractometer. Transmission electron microscopy (TEM) was used to study the structural-phase state of local regions of the test specimens. The foils were prepared using an ion thinning system JEOL Ion Slicer EM-09100IS designed to prepare specimens for research in scanning and transmission electron microscopes. The wear resistance of the modified specimens was studied on a high-temperature tribometer PC-Operated High Temperature Tribometer TNT-S-AX0000 and a three-dimensional non-contact profilometer Micro Measure 3D Station.

2. Results and discussion

High-intensity implantation of aluminum ions into a titanium specimen at a temperature 1170 K with an irradiation fluence of 10^{21} ions/cm^2 for one hour formed a deeply-doped layer with a thickness exceeding 150 μm with a maximum aluminum concentration near the surface of 19 at.% (Fig. 2). Detailed studies of the microstructure of titanium implanted under such conditions with aluminum are described in [37].

It has been established, that the implanted layer mainly consists of the α_2-Ti_3Al phase (97 vol.%). The formation of the intermetallic phase is also confirmed by TEM. The micro diffraction pattern analysis demonstrated the presence of α_2-Ti_3Al phase, where the grains are characterized by the 012, 122, 214, 310 orientation axes. It was shown that the grains of Ti_3Al have slightly elongated shapes, with an average size of 5 μm.

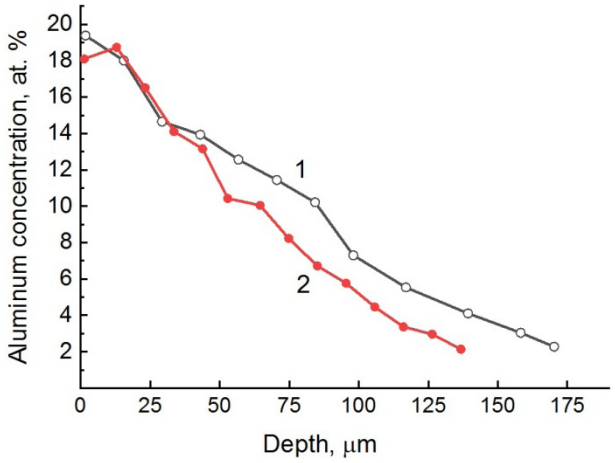

Fig. 2. Distribution profile of aluminum concentration over the titanium specimen depth:
1 – distribution of aluminum in titanium after high-intensity ion implantation; 2 – distribution of aluminum in titanium after exposure of the implanted sample to a powerful pulsed ion beam

Рис. 2. Профиль распределения концентрации алюминия по глубине титанового образца:
1 – после высокоинтенсивной ионной имплантации; 2 – после воздействия на имплантированный образец мощного импульсного ионного пучка

Post-implantation energy treatment with a powerful ion beam was carried out with two pulses with an ion current density on the target of 100 A/cm^2. Fig. 2 shows the distributions of aluminum dopant in titanium after high-intensity ion implantation (curve 1) and subsequent exposure of the surface to a powerful nanosecond ion beam (curve 2). The data in the figure show that after exposure of the sample to a nanosecond ion beam, both the width of the implanted layer and the maximum concentration of aluminum on the surface decrease. This effect can be explained by the fact that the action of a powerful ion beam is accompanied not only by the melting of the near-surface layer, but also by its partial evaporation. According to X-Ray phase analysis data (Fig. 3 and Table 1), it was found that the titanium alloy implanted with aluminum ions with subsequent energy impact consists of a solid solution based on Ti and Al. Basically, the matrix includes the $AlTi_3$, Ti_3Al and Al_2Ti phases, the individual Ti(h) and Al phases that have not reacted with each other are weakly expressed, and the Al_2O_3 phase is also weakly expressed.

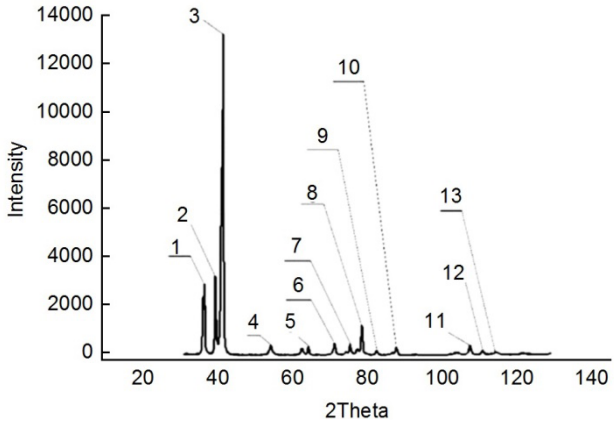

Fig. 3. X-ray of a titanium alloy implanted with aluminum ions

Рис. 3. Рентгенограмма титанового сплава, имплантированного ионами алюминия

Table 1. Phase composition of a titanium alloy implanted with aluminum ions

Таблица 1. Фазовый состав титанового сплава, имплантированного ионами алюминия

Peak № / Номер пика	Phase / Фаза	Lattice type / Тип решетки	Lattice parameters / Параметры решетки	d	h	k	l
1	$AlTi_3$	Hexagonal / Гексагональная	a: 5.755, c: 4.638	2.5	2	0	0
2				2.32	0	0	2
3	Al_2Ti	Tetragonal / Тетрагональная	a: 3.971, c: 2.432	2.23	0	1	9
4				1.69	0	1	13
5				1.47	0	1	14
6	Ti	Hexagonal / Гексагональная	a: 3.456, c: 5.525	1.31	2	0	2
7				1.25	1	0	4
8	Ti_3Al	Hexagonal / Гексагональная	a: 11.52, c: 4.65	1.2	3	3	3
9	Ti	Hexagonal / Гексагональная	a: 3.456, c: 5.525	1.16	2	0	3
10				1.1	2	1	1
11	Al	Cubic / Кубическая	a: 4.04	0.92	3	3	1
12				0.9	4	2	0
13	Al_2O_3	Rhombohedral / Ромбоэдрическая	a: 11.52, c: 4.65	0.9	4	2	0

Studies using transmission electron microscopy showed that the approximate depth of the layer modified by a powerful ion beam is ~4–4.5 μm. The change in the alloy structure confirms that the energy impact was carried out to a depth of 4.31 microns (Fig. 4).

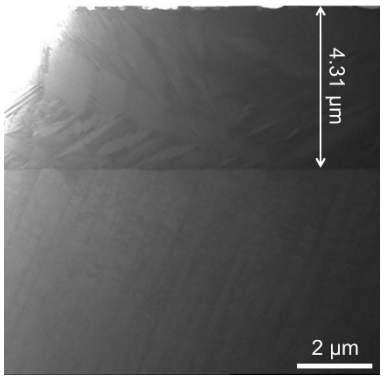

Fig. 4. TEM image of a titanium alloy implanted with aluminum ions

Рис. 4. ПЭМ изображение титанового сплава, имплантированного ионами алюминия

The near-surface layer of the specimen was studied by the TEM method, which was used to obtain bright-field and dark-field images, as well as a microdiffraction pattern of the specimen. When deciphering the microdiffraction pattern (Fig. 5), it was found that the alloy surface includes the Ti_3Al, Al_3Ti and Al_2Ti phases; traces of Al_2O_3 were also detected.

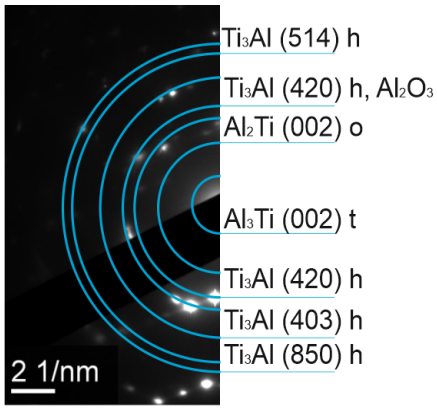

Fig. 5. Dark-field annular microdiffraction pattern of the surface of a titanium alloy implanted with aluminum ions, with deciphered phase composition

Рис. 5. Темнопольная кольцевая микродифракционная картина поверхности титанового сплава имплантированного ионами алюминия, с расшифрованным фазовым составом

According to the microdiffraction pattern identification, the Ti_3Al phases (Fig. 6) and the Al_3Ti (Fig. 7), Al_2Ti phases (Fig. 8) were localized in the bright-field image. The Ti_3Al phase is the main one and occupies the main volume. The particles of the Al_3Ti phase have a rounded shape. Particle sizes, on average, are in the range of 2–14 nm, the average size is 8.72 nm. The Al_2Ti phase is present in the specimen in a larger volume, and has the form of elongated bands, with a width of 4 to 60 nm, the length of phase precipitates in the test region is from 30 to 300 nm.

At a depth of 2 μm, the same phases were found as those on the modified specimen surface. Additionally, the $AlTi_2$ phase was identified. The Ti_3Al phase remains the main one, as that on the specimen surface (Fig. 9).

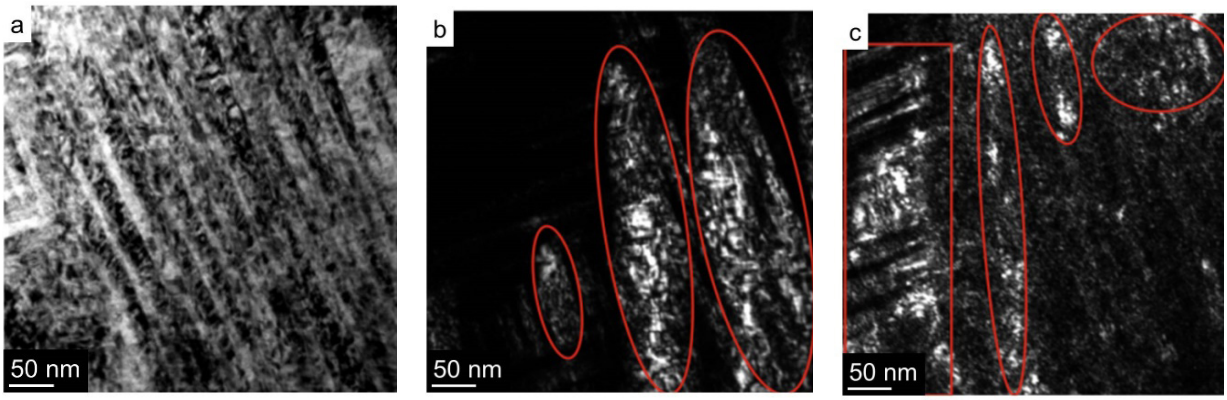

Fig. 6. TEM image:
a – original bright-field image; b, c – dark-field images with identified Ti_3Al phase

Рис. 6. ПЭМ изображение:
a – исходное светлопольное изображение; b, c – темнопольные изображения с идентифицированной фазой Ti_3Al

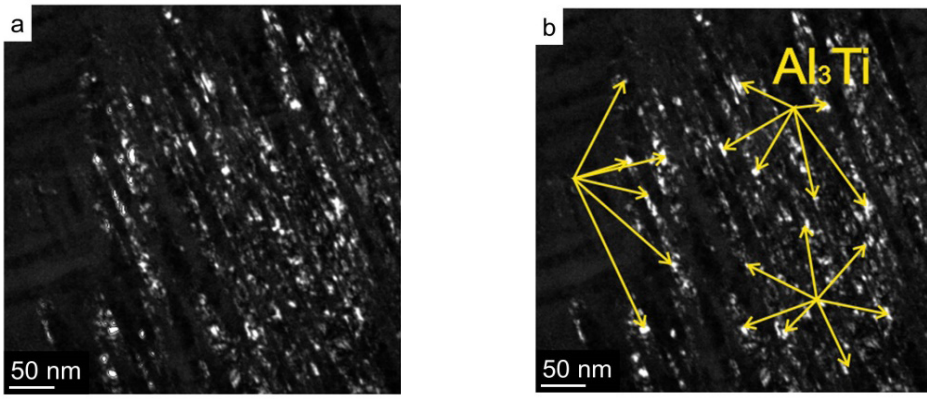

Fig. 7. TEM image:
a – original dark-field image; b – dark-field image with identified Al_3Ti phase

Рис. 7. ПЭМ изображение:
a – исходное темнопольное изображение; b – темнопольное изображения с идентифицированной фазой Al_3Ti

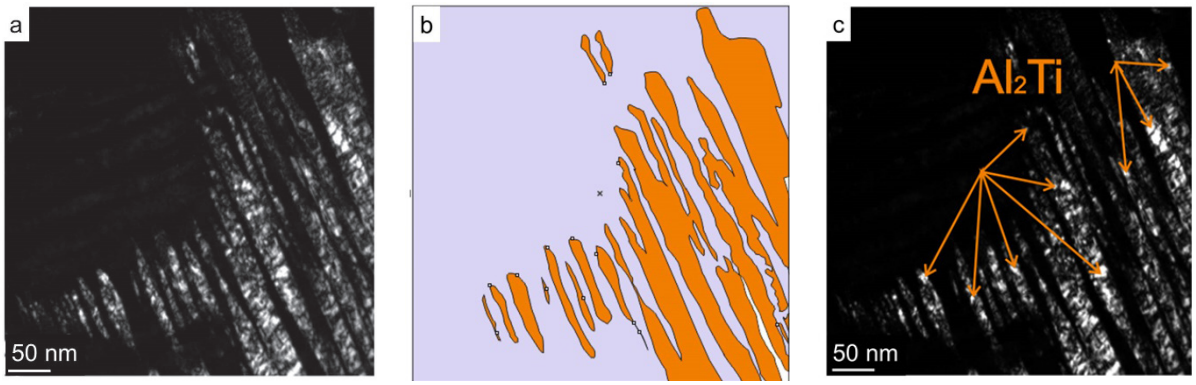

Fig. 8. TEM image:
a – original dark-field image; b – schematic localization of Al_2Ti phase;
c – dark-field image with identified phase

Рис. 8. ПЭМ изображение:
a – исходное темнопольное изображение; b – схематическая локализация фазы Al_2Ti;
c – темнопольное изображение с идентифицированной фазой

The Al_2Ti phase is localized in bands, as well as on the surface. The width of the bands is from 10 to 60 nm (average 34 nm); the length of the bands in the test region reaches 220–850 nm. For clarity of the general phase localization, a general scheme was made (Fig. 9).

When examining the area at a depth of 4 μm (Fig. 10), the deciphering of the annular dark-field diffraction patterns showed that the main phase is Ti_3Al with a hexagonal crystal lattice with parameters a = 1.15 nm, c = 0.46 nm. However, part of the reflexes also coincides with Al_2Ti phase with a tetragonal crystal lattice and lattice parameters: a = 0.39 nm and c = 2.4 nm.

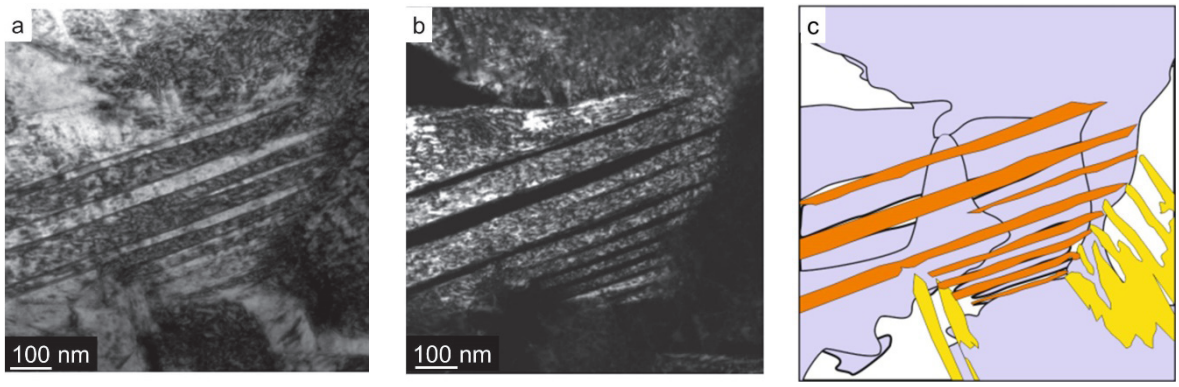

Fig. 9. TEM image:
a – original bright-field image; b – dark-field images; c – the general scheme of localization of the Ti_3Al, Al_3Ti and Al_2Ti phases.
Ti_3Al (purple colour), Al_3Ti (yellow) and Al_2Ti (orange)

Рис. 9. ПЭМ изображение:
a – исходное светлопольное изображение; b – темнопольные изображения;
c – общая схема локализации фаз Ti_3Al, Al_3Ti и Al_2Ti.
Ti_3Al (сиреневый цвет), Al_3Ti (желтый) и Al_2Ti (оранжевый)

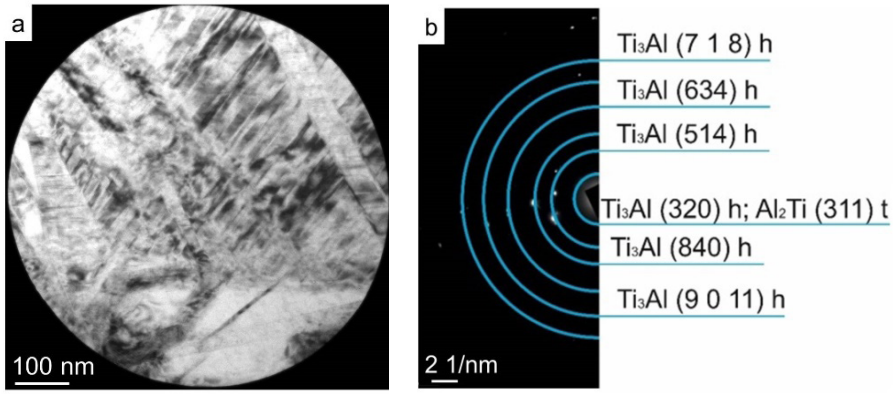

Fig. 10. TEM image:
a – bright-field image; b – dark-field point diffraction of the alloy, at a depth of 4 μm

Рис. 10. ПЭМ изображение:
a – изображение светлого поля; b – темнопольная точечная дифракция сплава, на глубине 4 мкм

When examining a region at a depth of 4.5 μm, it was found that the structure is monotonic. Deciphering of point dark-field diffraction patterns showed that the main phase at this depth is $AlTi_3$ with a tetragonal crystal lattice with parameters a = 0.38 nm, c = 0.85 nm. The average sizes of phase inclusions are from 100 to 200 microns (Fig. 11).

At a depth of 15 μm, the Ti_3Al, Al_3Ti, and Ti phases were identified. With increasing depth, the concentration of aluminum dopant decreases, which decreases the aluminum-containing phases. Fig. 12, *a* shows the microdiffraction pattern, with the deciphered phase composition. Ti_3Al phase remains the predominant phase. In Fig. 12, *b* the regions of $AlTi_3$ and Ti (t) phase precipitation are marked.

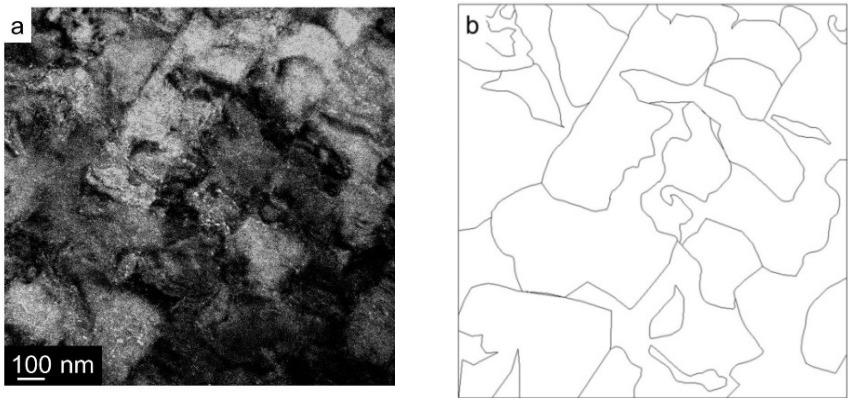

Fig. 11. Dark-field alloy at a depth of 4.5 μm:
a – TEM image of a titanium alloy implanted with aluminum ions at a depth of 4.5 μm; b – schematic representation of the grain structure

Рис. 11. Темное поле сплава на глубине 4,5 мкм:
a – ПЭМ-изображение титанового сплава, имплантированного ионами алюминия; b – схематическое изображение структуры зерна

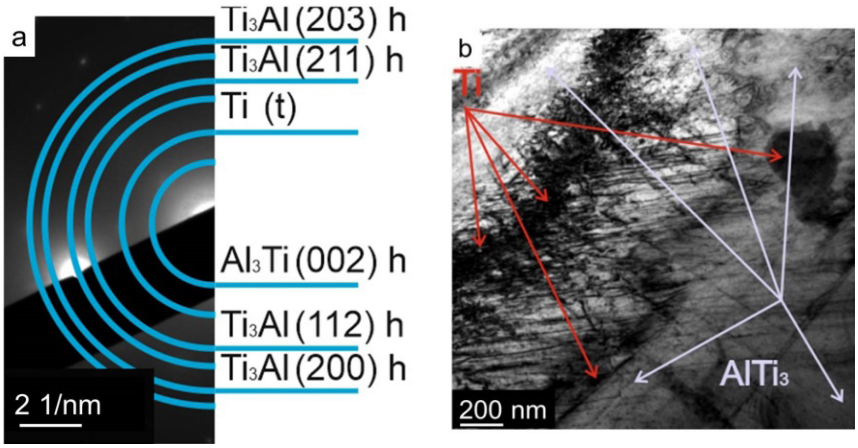

Fig. 12. Microdiffraction pattern with deciphered phase composition (*a*), TEM image with highlighted regions of phase localization (*b*)

Рис. 12. Микродифракционная картина с расшифрованным фазовым составом (*a*), ПЭМ-изображение с выделенными участками локализации фаз (*b*)

At a depth of 60 μm, the grain structure of the titanium alloy is visible, the average grain size is 250 μm (Fig. 13). Grain boundaries have thickness of up to 20 nm.

Fig. 14 shows data on the wear of the original titanium image, titanium implanted with aluminum ions and the specimen with subsequent energy impact by a powerful ion beam. Tribological studies have shown that post-implantation impact by a powerful pulsed beam improves wear resistance by 10 times compared to a titanium specimen modified with aluminum ions and by 18 times compared to the original titanium specimen.

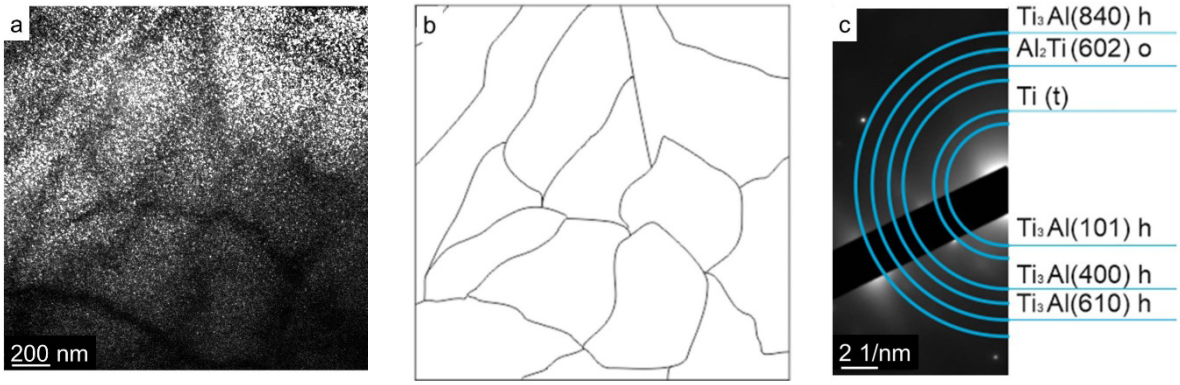

Fig. 13. TEM image of a titanium alloy implanted with aluminum ions at a depth of 60 μm (*a*), schematic representation of the grain structure (*b*), microdiffraction pattern with deciphered phase composition (*c*)

Рис. 13. ПЭМ изображение титанового сплава имплантированного ионами алюминия на глубине 60 мкм (*a*), схематическое изображение зеренной структуры (*b*), микродифракционная картина с расшифрованным фазовым составом (*c*)

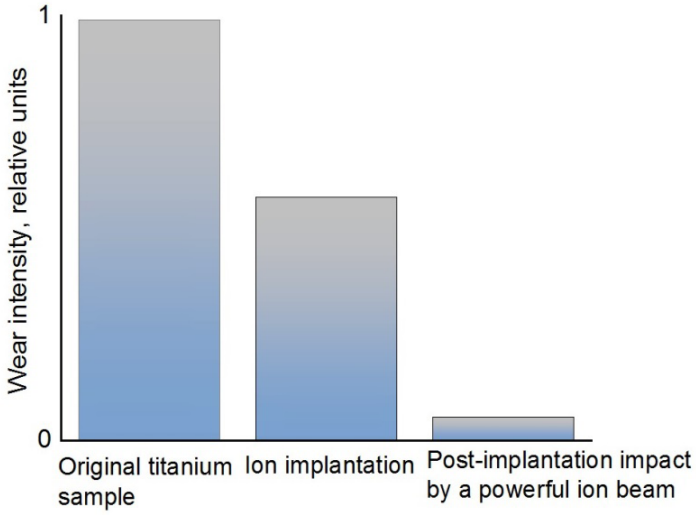

Fig. 14. Wear rate of a titanium specimen implanted with aluminum ions, a specimen with post-implantation impact by a powerful pulsed ion beam and the original titanium specimen

Рис. 14. Интенсивность износа образца титана имплантированного ионами алюминия, образца с постимплантационным воздействием мощного импульсного пучка ионов и исходного образца титана

Conclusions

Comparing the results of the present study of high-intensity implantation of aluminum ions into titanium with the data obtained in work [37], as well as a comparative analysis of the data obtained in this work at different depths of the ion-doped target layer, makes it possible to draw a number of important conclusions. The synergy of high-intensity ion implantation with post-implantation energy impact on the implanted surface of a pulsed ion beam with a high power density allows maintaining the depth distribution of the implanted dopant, but significantly changes the layer microstructure in the impact zone. Pulsed heating and repeated ultrafast cooling reduce the grain size due to heat transfer from the surface inside the material of the irradiated specimen. The synergy of deep doping of titanium with aluminum as a result of high-intensity ion implantation and the effect of super-fast hardening due to ultra-fast heat transfer increases the wear resistance of the surface layer by 18 times.

Acknowledgments / Благодарности

Исследование выполнено при финансовой поддержке Российского научного фонда, проект № 22-19-00051, https://rscf.ru/project/22-19-00051/.

The work was supported by the Russian Science Foundation, project № 22-19-00051, https://rscf.ru/project/22-19-00051/.

REFERENCES

1. Wang F., Khan A., Ayaz M., Ahmad I., Nawaz R., Gul N. Formation of intermetallic phases in ion implantation // J. Math. 2020. Article number 8875976. DOI: 10.1155/2020/8875976.

2. Komarov F. F., Yuvchenko V. N. Use of the temperature peak model for the description of track formation in semiconductor crystals irradiated by fast heavy ions // Technical Physics. 2003. V. 48, Iss. 6. P. 717–721. DOI: 10.1134/1.1583824.

3. Moncoffre N., Jagielski J. Redistribution of nitrogen implanted into iron: role of carbon and radiation defects // Surf. Coat. Technol. 1994. V. 65, Iss. 1–3. P. 30–36. DOI: 10.1016/S0257-8972(94)80005-7.

4. Hutchings R. A review of recent developments in ion implantation for metallurgical application //

Mater. Sci. Eng.: A. 1994. V. 184, Iss. 2. P. 87–96. DOI: 10.1016/0921-5093(94)91023-5.

5. Zhang L.-C., Chen L.-Y., Wang L. Surface Modification of Titanium and Titanium Alloys: Technologies, Developments, and Future Interests // Adv. Eng. Mater. 2019. V. 22, Iss. 5. Article number 1901258. DOI: 10.1002/adem.201901258.

6. Metel A., Grigoriev S., Melnik Y., Volosova M., Mustafaev E. Surface hardening of machine parts using nitriding and TiN coating deposition in glow discharge // Machines. 2020. V. 8, Iss. 3. Article number 42. DOI: 10.3390/MACHINES8030042.

7. Zatsepin D. A., Boukhvalov D. W., Zatsepin A. F., Mikhaylov A. N., Gerasimenko N. N., Zaporozhan O. A. Effect of long-term storage on the electronic structure of semiconducting silicon wafers implanted by rhenium ions // J. Mater. Sci. 2021.V. 56, Iss. 3. P. 2103−2112. DOI: 10.1007/s10853-020-05319-6.

8. Xie X., Chen C., Luo J., Xu J. The microstructure and tribological properties of M50 steel surface after titanium ion implantation // Appl. Surf. Sci. 2021. V. 564. Article number 150349. DOI: 10.1016/j.apsusc.2021.150349.

9. Rajput P., Kumar M., Singh U. B., Potdar S., Gome A., Reddy V. R., Bhattacharyya D., Jha S. N., Khan S. A. Singh F. Interface modification of Fe/Cr/Al magnetic multilayer by swift heavy ion irradiation // Surf. Interfaces. 2021. V. 26. Article number 101431. DOI: 10.1016/j.surfin.2021.101431.

10. Ryabchikov A. I., Sivin D. O., Bozhko I. A., Stepanov I. B., Shevelev A. E. Microstructure of titanium alloy modified by high-intensity implantation of low- and high-energy aluminium ions // Surf. Coat. Technol. 2020. V. 391. Article number 125722. DOI: 10.1016/j.surfcoat.2020.125722.

11. Jin J., Shao T. Effects of single- and dual-element ion implantation on tribomechanical properties of Cronidur 30 bearing steel // Surf. Coat. Technol. 2018. V. 344. P. 303–311. DOI: 10.1016/j.surfcoat.2018.03.033.

12. Nikmah A., Rudyardjo D. I., Ady J., Taufiq A. Studies on density, corrosion rate and hardness characteristics of stainless steel implanted by nitrogen ion // IOP Conf. Ser., Mater. Sci. Eng. 2019. V. 515, Iss. 1. Article number 012018. DOI: 10.1088/1757-899X/515/1/012018.

13. Ovchinnikov V. V., Uchevatkinai N. V., Kurbatova I. A., Lukyanenko E. V., Yakutina S. V. VT6 Titanium alloy wearability increase via implantation of copper and aluminum ions // Periodico Tche Quimica. 2019. V. 16, Iss. 32. P. 945–966. DOI: 10.52571/PTQ.v16.n32.2019.963_Periodico32_pgs_945_966.pdf.

14. Ghyngazov S. A., Kostenko V., Ovchinnikov V. V., Gushchina N. V., Makhinko F. F. Surface modification of corundum ceramics by argon ion beam // Inorganic Mater.: Appl. Res. 2019. V. 10. P. 438–444. DOI: 10.1134/S2075113319020199.

15. Ryabchikov A. I. Progress in low energy high intensity ion implantation method development // Surf. Coat. Technol. 2020. V. 388. Article number 125561. DOI: 10.1016/j.surfcoat.2020.125561

16. Sourani F., Enayati M. H., Ashrafizadeh F., Sayyedan F. S., Chu P. K. Enhancing surface properties of (Fe,Cr)Al–Al_2O_3 nanocomposite by oxygen ion implantation // J. Alloys Compounds. 2021. V. 853. Article number 156892. DOI: 10.1016/j.jallcom.2020.156892.

17. Yan Ch., Zeng Q., He W., Zhu J. Enhanced surface hardness and tribocorrosion performance of 60NiTi by boron ion implantation and post-annealing // Tribol. Int. 2021. V. 155. Article number 106816. DOI: 10.1016/j.triboint.2020.106816.

18. Poate J. M., Foti G., Jacobson D. C. Surface Modification and Alloying by Laser, Ion, and Electron Beams. Berlin: Springer, 2013. P. 414.

19. Wang D., Wang D., Yang Y., Guo T., Xiong X., Xie Y., Li K., Li B., Ghali M. Effect of pulse bias voltages on performance of CdTe thin film solar cells prepared by pulsed laser deposition // Sol. Energy. 2021. V. 213. P. 118–125. DOI: 10.1016/j.solener.2020.11.041.

20. Huang J. Study on tribological properties of 35CrMo steel after laser textured // Optik. 2021. V. 226, Part 1. Article number 165437. DOI: 10.1016/j.ijleo.2020.165437.

21. Li Y., Wu Y., Wang W., Lei M. Li X. Microstructure and mechanical properties of the Ni-B-Ti composite coating on TA_2 prepared by pre-plating and laser remelting // Surf. Coat. Technol. 2021. V. 405. Article number 126567. DOI: 10.1016/j.surfcoat.2020.126567.

22. Shulov V. A., Paikin A. G., Teryaev D. A., Bytsenko O. A., Engel'ko V. I., Tkachenko K. I. Structural-phase changes in surface layers of elements made of VT6 titanium alloy under irradiation by high-current pulsed electron beam // Inorganic Mater., Appl. Res. 2013. V. 4, Iss. 3. P. 189–192. DOI: 10.1134/S2075113313030118.

23. Ozur G. E., Proskurovsky D. I. Generation of low-energy high-current electron beams in plasma-anode electron guns // Plasma Phys. Rep. 2018. V. 44, Iss. 1. P. 18–39. DOI: 10.1134/S1063780X18010130.

24. Kaikanov M., Kozlovskiy A., Abduvalov A., Dukenbayev K., Zdorovets M. V., Tikhonov A. The use of pulsed beams for increasing radiation resistance of ceramics // J. Mater. Sci.: Mater. Electron. 2019. V. 30, Iss. 16. P. 15724–15733. DOI: 10.1007/s10854-019-01958-x.

25. Rej D. J., Rej D. J., Davis H. A., Olson J. C., Remnev G. E., Zakoutaev A. N., Ryzhkov V. A., Struts V. K., Isakov I. F., Shulov V. A., Nochevnaya N. A.,

Stinnett R. W., Neau E. L., Yatsui K., Jiang W. Materials processing with intense pulsed ion beams // J. Vac. Sci. Technol.: A. 1997. V. 15, Iss. 3. P. 1089–1097. DOI: 10.1116/1.580435.

26. Shulov V. A., Nochovnaya N. A., Remnev G. E., Pellerin F., Monge-Cadet P. High-power ion beam treatment application for properties modification of refractory alloys // Surf. Coat. Technol. 1998. V. 99, Iss. 1–2. P. 74–81. DOI: 10.1016/S0257-8972(97)00408-8.

27. Bandura N., Byrka O. V., Chebotarev V. V., Garkusha I. E., Makhlaj V. A., Medvedev V. Taran V. S., Tereshin V. I., Skoblo T. S., Pugach S. G. Alloying and modification of structural materials under pulsed plasma treatment // Intern. J. Plasma Environ. Sci. Technol. 2011. V. 5, No. 1. P. 2–6. DOI: 10.34343/ijpest.2011.05.01.002.

28. Uglov V. V., Cherenda N. N., Anishchik V. M., Stalmashonak A. K., Astashinski V. M. Mishchuk A. A. Formation of alloying layers in a carbon steel by compression plasma flows // Vacuum. 2007. V. 81, Iss. 10. P. 1341–1344. DOI: 10.1016/j.vacuum.2007.01.041.

29. Wei R. Low energy, high current density ion implantation of materials at elevated temperatures for tribological applications // Surf. Coat. Technol. 1996. V. 83, Iss. 1–3. P. 218–227. DOI: 10.1016/0257-8972(95)02828-5.

30. Wilbur P. J., Davis J. A., Wei R., Vajo J. J., Williamson D. L. High current density, low energy, ion implantation of AISI-M2 tool steel for tribological applications // Surf. Coat. Technol. 1996. V. 83, Iss. 1–3. P. 250–256. DOI: 10.1016/0257-8972(95)02830-7.

31. Williamson D. L., Ozturk O., Glick S., Wei R., Wilbur P. J. Microstructure of ultrahigh dose nitrogen-implanted iron and stainless steel // Nucl. Instrum. Methods Phys. Res.: B. 1991. V. 59–60, Part 2. P. 737–741. DOI: 10.1016/0168-583X(91)95693-8.

32. Wei R., Shogrin B., Wilbur P. J., Ozturk O. Williamson D. L., Ivanov I., Metin E. The Effects of Low-EnergyNitrogen-Ion Implantation on the Tribological and Microstructural Characteristics of AISI 304 Stainless Steel // J. Tribal. 1994. V. 116, Iss. 4. P. 870–876. DOI: 10.1115/1.2927347.

33. Wei R., Vajo J. J., Matossian J. N., Wilbur P. J., Davis J. A., Williamson D. L. Collins G. A. A comparative study of beam ion implantation, plasma ion implantation and nitriding of AISI 304 stainless steel // Surf. Coat. Technol. 1996. V. 83, Iss. 1–3. P. 235–242. DOI: 10.1016/0257-8972(95)02825-0.

34. Ryabchikov A. I., Sivin D. O., Ananin P. S., Ivanova A. I., Lopatin I. V., Korneva O. S., Shevelev A. E. High intensity, low ion energy implantation of nitrogen in AISI 5140 alloy Steel // Surf. Coat. Technol. 2018. V. 355. P. 129–135. DOI: 10.1016/j.surfcoat.2018.02.110.

35. Ryabchikov A. I., Kashkarov E. B., Shevelev A. E., Obrosov A., Sivin D. O. Surface modification of Al by high-intensity low-energy Ti-ion implantation: Microstructure, mechanical and tribological properties // Surf. Coat. Technol. 2019. V. 372. P. 1–8. DOI: 10.1016/j.surfcoat.2019.05.020.

36. Ryabchikov A. I., Sivin D. O., Bozhko I. A., Stepanov I. B., Shevelev A. E. Microstructure of titanium alloy modified by high-intensity implantation of low- and high-energy aluminium ions // Surf. Coat. Technol. 2020. V. 391. Article number 125722. DOI: 10.1016/j.surfcoat.2020.125722.

37. Ryabchikov A. I., Ananin P. S., Dektyarev S. V., Sivin D. O., Shevelev A. E., High intensity metal ion beam generation // Vacuum. 2017. V. 143. P. 447–453. DOI: 10.1016/j.vacuum.2017.03.011.

38. Brown I. G. (ed.). The physics and technology of ion sources. USA: John Wiley and Sons, Inc, 1989. P. 396.

39. Remnev G. E., Isakov I. F., Opekounov M. S., Matvienko V. M., Ryzhkov V. A., Struts I. I. Grushin A. N., Zakoutayev A. V., Potyomkin V. A., Tarbokov A. N., Pushkaryov V. K., Kutuzov V. L., Ovsyannikov M. Yu. High intensity pulsed ion beam sources and their industrial applications // Surf. Coat. Technol. 1999. V. 114, Iss. 2–3. P. 206–212. DOI: 10.1016/S0257-8972(99)00058-4.